



# Influence of pillar wide and room's height on the acoustic emission phenomena during crack evolution

Amir Rezaei · Vahab Sarfarazi · Nima Babanouri ·  
Mohammad Omid manesh · Reza Bahrami ·  
Xiao Wang

Received: 17 December 2021 / Accepted: 12 December 2023  
© The Author(s) 2023

**Abstract** The present study probes the effects of pillar wide and room's height on the failure mechanism of model using experimental test and numerical simulation. For this purpose, firstly gypsum specimens with dimension of 15\*15\*5 cm containing two neighboring rooms and one pillar were prepared. Pillar widths were 3 cm, 6 cm and 9 cm. In each pillar width, the roof height was 1 cm, 2 cm, 3 cm, 4 cm, 5 cm, and 6 cm. Totally 9 physical specimens were tested. Concurrent with experimental tests, 18 numerical models were simulated. The results show that the pillar wide and roof height affect the failure pattern and compressive strength of models. Two different failure patterns were observed in the model. In the first stage, two tensile fractures were developed from room edge and propagated parallel to loading axis till coalescence with model boundary. In the second

stage, mixed tensile-shear cracks were developed through the rock pillar. It is shown that with the augment of stress-strain curve until the peak, the AE hits of numerical specimens presents three stages. In the first stage, AE hits is almost zero; this step is in the elastic stage, and there isn't any crack in the sample. In the second stage, AE hits is in a slowly increasing stage, which is due to the micro cracks in the model continuous expansion. In the third stage, the AE hits increase rapidly, because the rock almost enters its bearing limit and the crack propagation speed is very fast. Generally, the maximum value of AE is near the peak value. When the roof height is the same, different pillar wide led to a significant change in the maximum AE hits. The experimental test and numerical simulation show the similar outcomes.

A. Rezaei · M. Omid manesh  
Hamedan University of Technology, Hamedan, Iran

V. Sarfarazi (✉) · N. Babanouri  
Mining Engineering Department, Hamedan University  
of Technology, Hamedan, Iran  
e-mail: Sarfarazi@hut.ac.ir

R. Bahrami  
Department of Civil Engineering, Beyza Branch, Islamic  
Azad University, Beyza, Iran

X. Wang  
College of Mining and Safety Engineering, Shandong  
University of Science and Technology, Qingdao 266590,  
People's Republic of China

## Article Highlights

1. Investigation of the influence of pillar dimension on the failure mechanism of rock pillar shows that in constant pillar wide, the mixed mode failure change to pure tensile failure by increasing the pillar height.
2. In constant pillar height, the mixed mode failure change to pure tensile failure by decreasing the pillar wide.
3. Delay failure in rock pillar changes to rapidly failure by increasng the ratio of pillar height to pillar wide.

4. In constant pillar height, acoustic emission phenomena was increased by decreasing the pillar wide while in constant pillar wide, acoustic emission phenomena was increased by increasing the pillar height.

**Keywords** Immediate roof · Axial loading · Edge notch · PFC

## 1 Introduction

One of the important issues in underground mining, is design of pillars. Issues such as pillars size, pillar strength, condition of coal seam cracking, mining depth, condition of floor and roof strata and stress distribution in a coal pillar have major effect on the coal burst phenomena. Of these parameters, coal pillar width and its height are adjustable and thus can be utilized to control the coal burst hazard level of the mining area. The pillar design is important in optimization of the mining operations. The mechanical behaviour of the mine pillar and the surrounding environment must be studied to achieve an economical and safe design of the pillars (Bogert et al 1997). Brady et al. (1985), proposed a pillar strength mathematical relation accounting for pillar dimension and geometry to reduce the pillar burst. Bieniawski 1968 reported that by augmenting the size and achieving an approximate amount at a cube size of near 1.5 m which based on his opinion, was the critical size for coal, the compressive strength of coal cubes (short-term strength) declined. The effect of confinement on rock pillar strength was investigated by Lunder and Pakalnis (1998). Gonzalez-Nicieza et al (2006), formulated a new relation based on Bieniawski's rock mass quality classification and the shear-resistance safety factor of pillars to increase the pillar stability. Esterhuizen (2006), studied on several factors which affects the pillar strength at low width-to-height ratios in hard brittle rock and implied that the strength of narrow pillars was more variable than wider ones. Mortazavi et al. (2009), declared at high WH ratios, pillars show a very stiff behavior in the elastic zone, representing a high load-bearing capacity. Ghasemi and Shahriar (2012), suggested a novel coal pillar design approach for decreasing the coal burst phenomena. Suorineni and Kaiser (2011) and Suorineni

et al. (2014), introduced pioneer approach to the topic of why pillars in ore bodies in shear are more talented to disastrous failures than would typically be anticipated. Liu and Xu (2000), calculated rock mass strength for the gob zone of a phosphate mine with respect to rock mass classification, analyzed stability of pillars in the gob zone utilizing the safety factor and reliability analysis methods, and demonstrated the safety factor of pillars by the mean safety factor. Yang (2005), suggested a novel design method for pillar spacing, which has been employed efficiently in practical goals of engineering. Wang and Li (2010), introduced the approach of shear-resistance safety factor for mine pillars, taking into account that pillars ordinarily failed in shear and proposed that pillars are secure and reliable when the shear-resistance safety factor is higher than 1.2. Wang et al. (2012), developed a numerical relation for pillar width for deepstoping mining and proposed the depth and stopping span are the decisive parameters which impressed the appropriate pillar width. In short, appropriate pillar design is the pivotal factor to avoidance coal burst and diminution of associated accidents (Ghasemi 2014; Li 2005; Zhong 2012; Liu 2021). Murali Mohan et al. (2001) was investigated the effect of pillar wide on the coal burst in Indian coal mines by using FLAC3D. Chen et al. (1997), studied on the influences of rock pillar width on the stability behavior of three and four parallel tunnels during excavation, numerally. They found that in addition to the tunnel cross section and geological conditions, the rock pillar widths also have a pivotal role on interaction effects. Furthermore, Chen et al. (2009) and Kaiser and Tang (1998), presented a double-rock sample model for investigating the pillar rockburst process and simulation of the progressive failure pattern in a

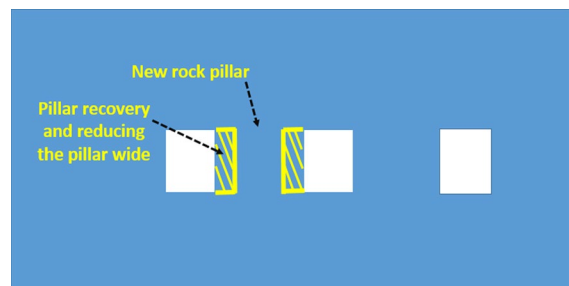


**Fig. 1** Reducing of the pillar diameter due to its recovery

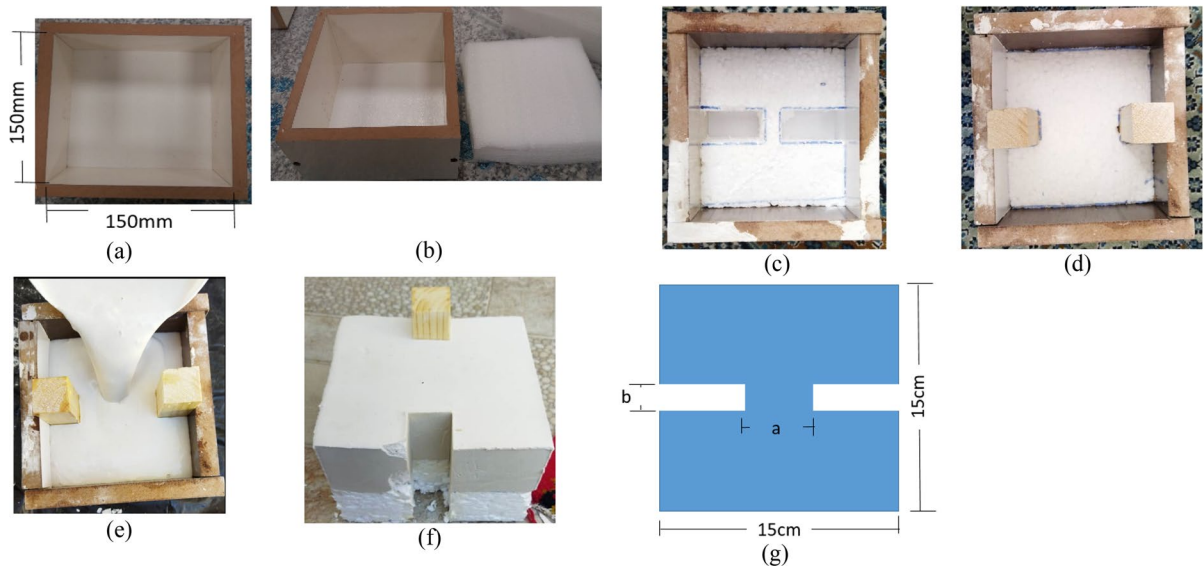
pillar. Li (2020), studied the influence of size of pillar on distribution of plastic zone, stress redistribution, and roof stability of deep mining. It reveals how shape of surrounding rock plastic zone was affected by size of the pillar. Gao (2018) and Qiu et al. (2019) studied the behavior of rock pillars under uniaxial compression. They found that pillar dimensions have important effect on the failure pattern of rock pillar. Some researchers revealed that with the increase of coal pillar width, the stress concentration shifted from the solid coal laterally to the middle of pillar (Liu et al. 2021, Jin 2018; Zhang et al. 2018). Sun et al. (2019) and Fan et al. (2019), investigated the rules of the stress redistribution in pillars under various dip angles and buried depth. When the dip angle of coal seam increased, the extent of stress concentration was more apparent. In the previous research, the effect of the reducing of pillar diameter due to its recovery was neglected on the room stability (Fig. 1). Also, the effect of variation of the pillar height was ambiguous on the crack initiation threshold.

Therefore in this study, the variation of both of the pillar wide and pillar height have been investigated on the crack evolution and acoustic emission phenomena (AE) under axial loading. The experimental test and particle flow code (PFC) were utilized to simulate pillars

of varied dimensions and to study the failure mechanisms. The fracture process and damage were assessed by AE methods. The simulation outcomes pave the way to attain more comprehensive knowledge about pillar mechanics and can be employed for more secure design and development of underground mine pillars.

## 2 Physical testing of rock-like samples containing rooms and pillars










For the purpose of simulating the room and pillar, rock-like materials were used in the experiments. The materials were blended and a mixture of gypsum to water with a weight ratio of 1.2 to 1 gypsum to water was provided. Gypsum is the material that employed in current research, the identical material utilized in (Reyes et al. 1991; Shen et al. 1995; Bobet et al. 1998; Takeuchi 1991). For selecting gypsum, there are four proofs: first of all, besides being a weak rock, gypsum is an ideal rock with which to represent a wide range of soft rocks; next, whole of former experience and outcomes can be utilized, and the former discoveries can be contrasted with the new ones; third, this permit for a huge amount of samples to be prepared effortlessly; and the final reason, iteration of outcomes.



**Fig. 2 a** The frame with dimensions of 150 mm×150 mm×100 mm, **b** and **c** a unique plastic fiber with a dimension of 150 mm×150 mm×50 mm was put into the frame, **d** the wooden mold within the plastic fiber, **e** slurry

within the box, **f** the steel molds were taken out from the mold, **g** Room and pillar with different dimension pillar wide “a” and roof height “b”

**Table 1** Room and pillar with different dimension

Room height (cm)	Pillar length (cm)		
	9	6	3
1	 (a)	 (b)	 (c)
2	 (d)	 (e)	 (f)
3	 (g)	 (h)	 (i)

Gypsum is representative of soft rock pillar such as coal rock reported by Qu et al. (2021). The mold dimensions were  $150 \times 150 \times 100$  mm (Fig. 2a). One plastic foam with dimensions of  $150 \times 150 \times 50$  mm was situated inside the mold (Fig. 2b and c). For producing the room, two rectangular wooden molds were inserted inside the plastic foam (Fig. 2d). Wooden mold lengths were 3 cm, 4.5 cm and 6 cm. wooden mold thicknesses were 1 cm, 2 cm and 3 cm. Their height was 170 mm. These elements were lubricated by oil and then the mixture was poured inside the mold (Fig. 2e). The elements were removed after the initial hardening of the sample (Fig. 2f). All models consisted of two rooms. Figure 2g shows the schematic view of specimens. “a” and “b” are pillar length and room height, respectively (a=3 cm, 4.5 cm

**Fig. 3** Electro hydraulic universal testing machine

and 6 cm,  $b=1$  cm, 2 cm and 3 cm). Nine different model with different room dimension were prepared (Table 1). The samples were preserved in dry and cool circumstances for 28 days. In order to increase the reliability of the test and eliminate accidental errors, three test blocks with similar were provided for every set.

### 2.1 Testing the samples

The electro hydraulic universal testing apparatus was employed in order to perform uniaxial compression tests on samples. Experimental system consists of a test bed, control system, and data logger (Fig. 3). The

rate of loading displacement was set to 0.05 mm per minute.









### 2.2 Failure behavior in laboratory testing

#### 2.2.1 Failure pattern

(a) Room height was 1 cm.

When pillar wide was 3 cm (Table 2a), two different failure patterns were observed in the model. In the first stage, one tensile fracture was initiated from room edge and propagated horizontally till

**Table 2** Failure pattern in samples with different pillar wide and roof height

Room height (cm)		Pillar length (cm)		
		3	6	9
1	1	 (a)	 (b)	 (c)
	2	 (d)	 (e)	 (f)
	3	 (g)	 (h)	 (i)



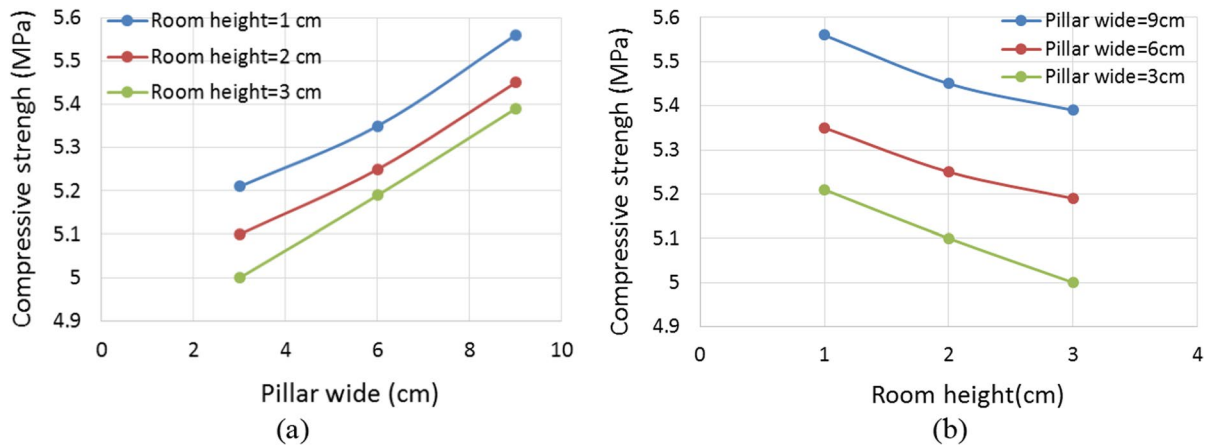


**Fig. 4** Effect of roof thickness on the compressive strength for different models

coalescence with other room edge. In the second stages, two tensile fractures were developed from room edge and propagated vertically till coalescence with sample boundary. These patterns were observed for two other pillar wide of 6 cm (Table 2b) and 9 cm (Table 2c). The failure intensity decreased by increasing the pillar wide.

(b) Room height was 2 cm.

When pillar wide was 3 cm (Table 2d), two different failure patterns were observed in the model. In the first stage, one tensile fracture was initiated from room edge and propagated horizontally till coalescence with other room edge. In the second stages, two tensile fractures were developed from room edge and propagated vertically till coalescence with sample boundary. These patterns were observed for two other pillar wide of 6 cm (Table 2e) and 9 cm (Table 2f). The failure intensity decreased by increasing the pillar wide.

(c) Room height was 3 cm.

When pillar wide was 3 cm (Table 2g), two different failure patterns were observed in the model. In the first stage, one tensile fracture was initiated from room edge and propagated horizontally till coalescence with other room edge. In the second stages, two tensile fractures were developed from room edge and propagated vertically till coalescence with sample boundary. These patterns were observed for two other

pillar wide of 6 cm (Table 2h) and 9 cm (Table 2i). The failure intensity decreased by increasing the pillar wide.

By comparison between failure patterns of specimens with different room height, it could be concluded that the failure intensity increased by increasing the rooms height.

2.2.2 *The influence of pillar length and room height and notch angle on the compressive strength*

Figures 4a show the effect of pillar wide on the compressive strength of model for various room heights i.e. 1 cm, 2 cm and 3 cm. totally, the compressive strength was increased by increasing the pillar wide. Figures 4b show the effect of room height on the compressive strength of model for various pillar wide i.e. 3 cm, 6 cm and 9 cm. totally, the compressive strength was declined by enhancing the room height.

### 3 Numerical model

#### 3.1 Particle flow code

Potyondy (2012), proposed a flat joint (FJ) model based on the particle's polygonal grain structure. The contact of FJ is depicted as locally flat conceptual surfaces centered at the area of contact and attached stiffly to a piece of particle. Each piece has a face, which is its notional surface and it is in interaction with the contacting piece face. Thus, all faced grains

are shown as a circular or spherical core with skirted faces. The shape of faces is disk or line (in 2D). The particle assembly bonded by FJ contacts is named FJM (flat-jointed material). The boundary between faced grains is discretized inside elements which can be bonded or unbonded. Then FJ was installed at a contact of grain–grain and force and torque at each element are set to zero and were updated according to the force–displacement law of bond and faces relative motion. The shear and normal force was updated in incremental and direct mode, respectively. As long as the strength does not exceed its limit, the behavior of the bonded element remains linear elastic (Potyondy 2015, 2017).

### 3.2 Preparation and calibration of PFC2D model for rock-like material

For current research, providing the test model was based on the standard process of producing a PFC2D assembly, Potyondy and Cundall (2004), entirely described this process. The process includes

producing particles, particle compression, installation of isotropic stress (initialization of stress), particle floatation (floaters), removing and installation of bonds. Because of the small sizes of samples, effect of gravity and the influence of gravity-induced stress gradient on the macroscopic behavior are negligible. Uniaxial compressive strength and Brazilian test were used to calibrate Particle’s characteristics and flat joint model. Based on micro-characteristics presented in Table 3 and methods of standard calibration (Sarfrazi et al. 2021), an assembly of calibrated PFC particles was generated. The experimental uniaxial compression test and numerical simulation are shown in Fig. 5a and b, respectively. In addition, experimental Brazilian test and numerical simulation are depicted in Fig. 5c and d, respectively. The outcomes showed fine matching between numerical simulation and experimental test. Furthermore, as listed in Table 4 the characteristics of specimen samples -obtained from the numerical models such as elastic modulus, Poisson’s ratio, UCS values- are approximately identical to the experimental amounts.

**Table 3** Micro characteristics used to introduce the intact rock

Particle micro properties		Flat-joint micro properties	
Model height (mm)	108	Gap ratio	0.5
Model width (mm)	54	Ec (GPa)	0.3
Kn/ks	1.7	Bonded friction	0.83
Density (kg/m <sup>3</sup> )	2500	Tensile strength	0.1
Minimum particle diameter (mm)	0.54	Tensile strength standard deviation (MPa)	0.01
Maximum particle diameter	1.08	Cohesion (MPa)	0.5
Ec(GPa)	0.3	Cohesion standard deviation (MPa)	0.05
Porosity	0.08	Number of elements	2
		Kn/ks	1.7

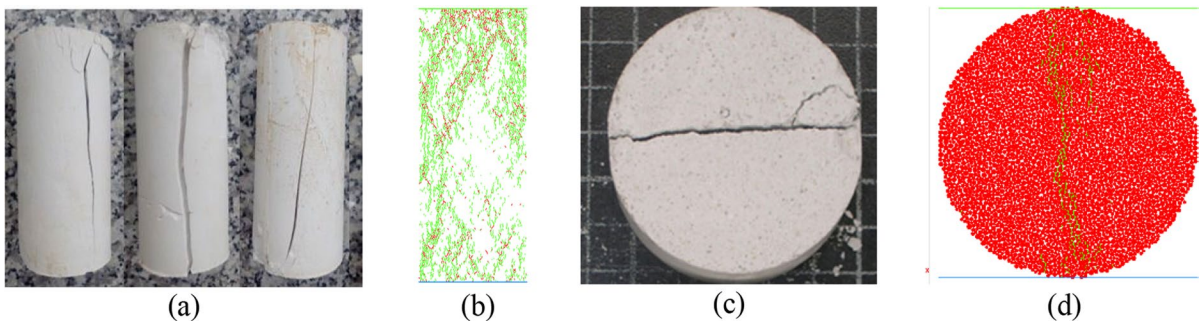


**Fig. 5** a Test of experimental compression, b Test of numerical compression, c Test of experimental Brazilian and d Test of numerical Brazilian

**Table 4** Comparison of macro-mechanical characteristics between model and experiments

Mechanical characteristics	Experimental results	PFC2D Model results
Elastic modulus, (GPa)	5	5
Poisson's ratio	0.18	0.19
UCS, (MPa)	7.4	7.4
Brazilian tensile strength (MPa)	1	1.05

### 3.3 Numerical compressive tests

First, PFC2D was calibrated. Then, by composing a box model in the PFC2D, researchers simulated uniaxial tests for pillar, numerally. The dimensions of the PFC sample were 150 mm×150 mm. The box sample included a number of 13,629 disks and the minimum radius of 0.27 mm.

Two rooms were created by removing the particles from the model (Table 5). To investigate the effect of pillar width (W) and pillar height (h) on the failure mechanism of rock pillar, w/h ratios changed from 0.5 to 9. Different ratios of pillar wide (W) to pillar height (H) were depicted in Table 5. The room's dimensions were (c\*d in Table 5a) 1 cm\*3 cm, 1 cm\*4.5 cm, 1 cm\*6 cm, 2 cm\*3 cm, 2 cm\*4.5 cm, 2 cm\*6 cm, 3 cm\*3 cm, 3 cm\*4.5 cm, 3 cm\*6, 4 cm\*3 cm, 4 cm\*4.5 cm, 4 cm\*6, 5 cm\*3 cm, 5 cm\*4.5 cm, 5 cm\*6, 6 cm\*3 cm, 6 cm\*4.5 cm, 6 cm\*6. Horizontal distance between two rooms (pillar wide) change from 3 to 9 cm with increment of 3 cm. 18 different models containing room and pillar were prepared (Table 5).

There are two walls at the bottom and top of the model. Top and bottom walls were moved toward the each other so axial force was applied on the model. The rate of axial load on the model was 0.05 mm per minute and the compression force was recorded by registering the reaction forces on the top wall.

It is important to note that model configuration and experimental configuration were identical for room dimensions of 1 cm\*3 cm, 1 cm\*4.5 cm, 1 cm\*6 cm, 2 cm\*3 cm, 2 cm\*4.5 cm, 2 cm\*6 cm, 3 cm\*3 cm, 3 cm\*4.5 cm and 3 cm\*6 cm (Tables 1 and 5). Whereas there is not any geometrical variation in third dimension, therefore it is possible to simulate the mechanical behavior of rock pillar two dimensionally.

### 3.4 Failure mechanism of numerical models

#### 3.4.1 Bond force distribution before the crack initiation

(a) Constant wide of pillar and different room height.

Figure 6 shows the distribution of bond force within the modelled samples before the initiation of crack under far field stress of 1 MPa (pillar wide was constant=3 cm and room height were different). In Fig. 8, the black and red lines illustrate the vectors of compression and tensile force in the model, respectively. The thick lines and their accumulation show the spaces where bigger forces are applied on the model. It is indicated that at the tensile force was concentrated near the pillar walls and compressive force was concentrated middle of the pillar. Under far field stress of 1 MPa, the concentration of maximum tensile force near the room walls with height of 1 cm was 1500 N while it was 2250 N in room with height of 6 cm. in other word, concentration of maximum tensile force was increased by increasing the room height. Therefore by increasing the room height, the pillar failure was occurred in lower far field stress. The similar trend was occurred for other pillar wide.

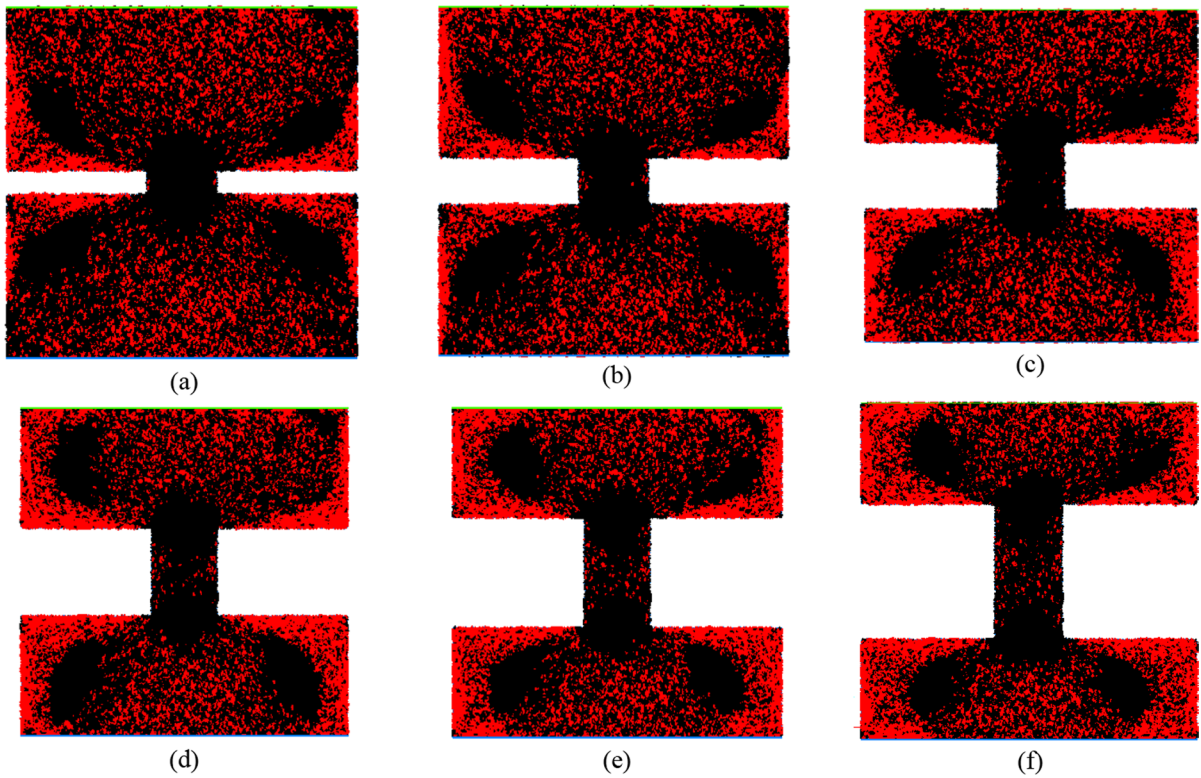
(b) Constant height of room and different pillar wide.

Figure 7 show distribution of bond force within the modelled samples before the initiation of crack under far field stress of 1 MPa (room height was constant=4 cm and pillar wide were different). The black and red lines in Fig. 7 introduce the vectors of compression and tensile force in the model, respectively. The areas where larger forces are applied on the model, represented by thick lines and their accumulation. It is depicted that at the tensile force was concentrated near the pillar walls and compressive force was concentrated middle of the pillar. Under far field stress of 1MPa, the concentration of maximum tensile force near the room walls pillar wide of 3 cm was 1950 N while it was 1690 N in pillar with wide of 9 cm. in other word, concentration of maximum tensile force was decreased by increasing the pillar wide.



**Table 5** Room and pillar with different dimension

Pillar height (H) (cm)	Pillar wide (W) (cm)		
	3	6	9
1	 <p>(W/H)=3 (a)</p>	 <p>(W/H)=6 (b)</p>	 <p>(W/H)=9 (c)</p>
2	 <p>(W/H)=1.5 (d)</p>	 <p>(W/H)=3 (e)</p>	 <p>(W/H)=4.5 (f)</p>
3	 <p>(W/H)=1 (g)</p>	 <p>(W/H)=2 (h)</p>	 <p>(W/H)=3 (i)</p>
4	 <p>(W/H)=0.75 (a)</p>	 <p>(W/H)=1.6 (b)</p>	 <p>(W/H)=2.25 (c)</p>
5	 <p>(W/H)=0.6 (d)</p>	 <p>(W/H)=1.2 (e)</p>	 <p>(W/H)=1.8 (f)</p>
6	 <p>(W/H)=0.5 (g)</p>	 <p>(W/H)=1 (h)</p>	 <p>(W/H)=1.5 (i)</p>



**Fig. 6** Compressive and tensile force distribution of in model with pillar wide of 3 cm and room height of, **a** 1 cm, **b** 2 cm, **c** 3 cm, **d** 4 cm, **e** 5 cm and **f** 6 cm

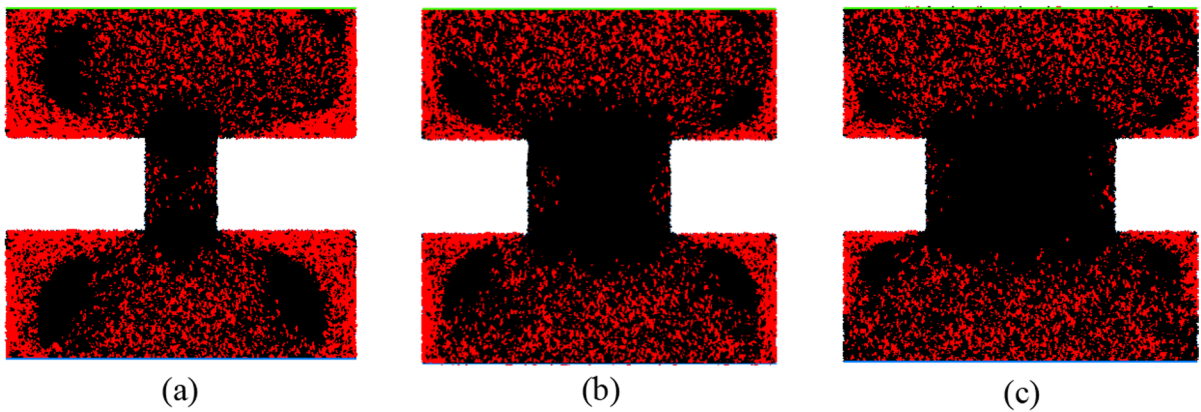


**Fig. 7** Compressive and tensile forces distribution in the model with room's height of 4 cm and pillar's width of **a** 3 cm, **b** 4.5 cm, **c** 6 cm

Therefore by increasing the pillar wide, the pillar failure was occurred in higher far field stress. The similar

trend was occurred for other pillar wide. The similar trend was occurred for other room height.

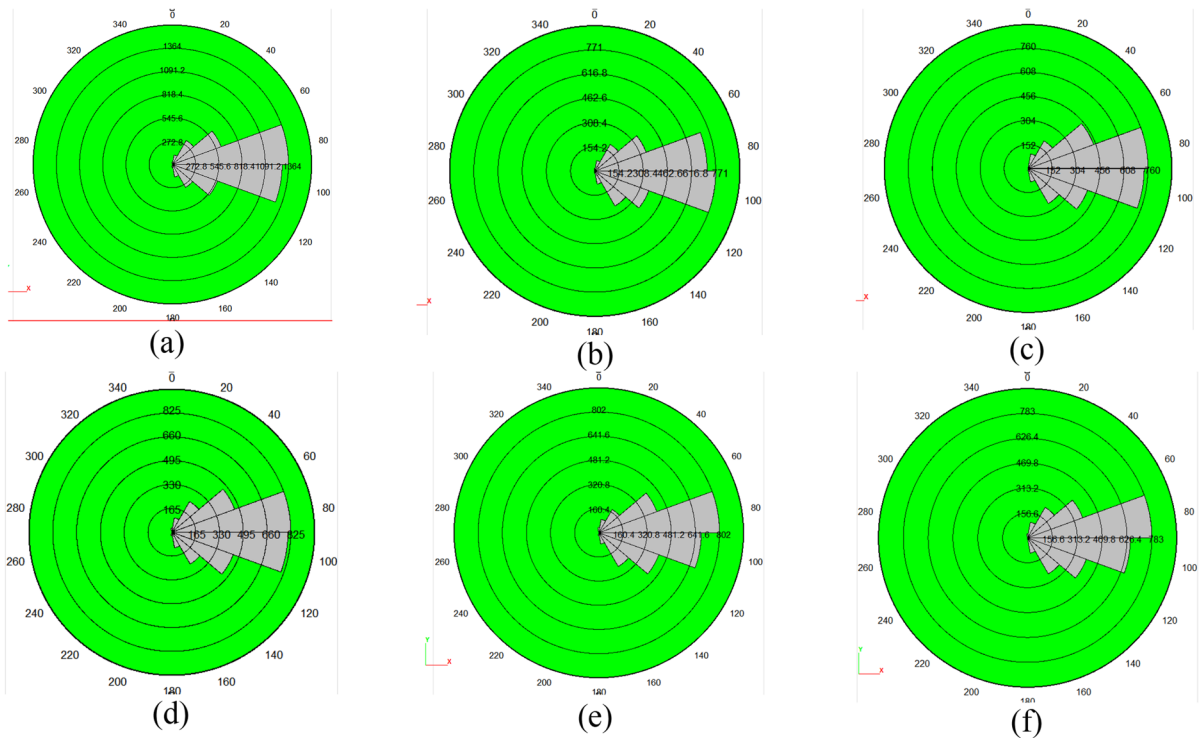


**Fig. 8** Rose diagram of crack development for pillar wide of 3 cm and rooms height of **a** 1 cm, **b** 2 cm, **c** 3 cm, **d** 4 cm, **e** 5 cm and **f** 6 cm

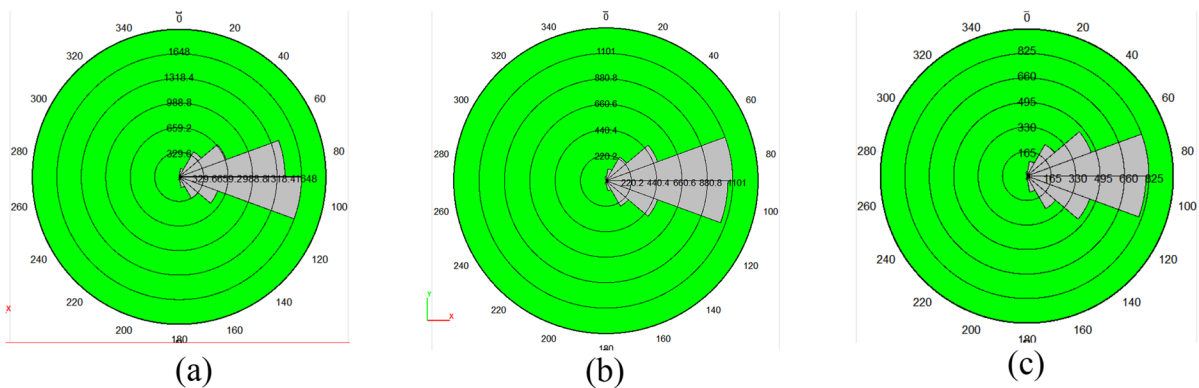


**Fig. 9** Rose diagram of crack development for room's height of 4 cm and pillar's width of **a** 3 cm, **b** 6 cm, **c** 9 cm

**3.4.2 Effects of pillar wide and room height on the Ross diagram of crack growth**

Figure 8 represents Ross diagram of crack development for pillar wide of 3 cm and different room's height i.e. 1 cm, 2 cm, 3 cm, 4 cm 5 cm and 6 cm. In all the configurations, the angles of micro cracks

changed from 75 to 105 degrees which signifies that the variations of room's height has not any effect on the fracture angle.

Figure 9 shows Ross diagram of crack development for room's height of 4 cm and different pillar wide i.e. 3 cm, 6 cm, 9 cm. In all the configurations, the angles of micro cracks varied from 75 to 105

degrees which means that the variations of pillar's width has not influence on the fracture angle.

### 3.4.3 Failure pattern

Table 6 represents the failure pattern of numerical model. Black and red lines illustrate the tensile and shear crack, respectively.

#### (a) Rooms height was 1 cm.

When pillar wide was 3 cm (Table 6a), two different failure patterns were observed in the model. In the first stage, two tensile fractures were developed from room edge and propagated parallel to loading axis till coalescence with model boundary. In the second stage, mixed tensile-shear cracks were developed through the rock pillar. These patterns were observed for two other pillar wide of 6 cm (Table 6b) and 9 cm (Table 6c). The failure intensity decreased by increasing the pillar wide.

#### (b) Rooms height was 2 cm.

When pillar wide was 3 cm (Table 6d), four tensile cracks were developed from roof of the rooms and two tensile fractures were developed from room edge. Also, mixed tensile-shear cracks were developed through the rock pillar. These patterns were observed for two other pillar wide of 6 cm (Table 6e) and 9 cm (Table 6f).

#### (c) Rooms height was 3 cm.

When pillar wide was 3 cm (Table 6g), four tensile cracks were developed from roof of the rooms and two tensile fractures were developed from room edge. Also, mixed tensile-shear cracks were developed through the rock pillar. These patterns were observed for two other pillar wide of 6 cm (Table 6h) and 9 cm (Table 6i).

#### d) Rooms height were 4 cm, 5 cm and 6 cm.

When pillar wide was 3 cm (Table 6j, m, p), four tensile cracks were developed from roof of the rooms and two tensile fractures were developed from room edge. Also, mixed tensile-shear cracks were developed through the rock pillar. These patterns were observed for two other pillars width of 6 cm (Table 6k, n, q) and 9 cm (Table 6l, o, r). The shear

bands were developed in the model by increasing the pillar wide.

By comparison between failure patterns in Table 6, it could be concluded that in constant pillar wide, the shear cracks increased in the model by increasing the room's height. Also, in constant room's height, the shear bands developed in the model by increasing the pillar wide.

By comparison between Tables 2 and 6a–i, one can observe that the failure pattern is the same for the laboratory experiments and numerical modeling. The more propagating of tensile cracks in numerical models were due to continuing the model loading after post peak failure stress while the experimental test was stopped in peak failure stress.

### 3.4.4 Stress–strain curve across with the total crack number and acoustic emission characteristics for different models

#### (a) Room height was 1 cm.

Figure 10a, c, e show the stress–strain curve across with the total crack number for pillar wide of 3 cm, 6 cm and 9 cm, respectively (room height of 1 cm). Figure 10b, d, f shows the stress–strain curve across with AE hits for pillar wide of 3 cm, 6 cm and 9 cm, respectively. The reason why we analyze the acoustic emission characteristics (AE hits) of rock pillar in the process of compression is that the engineering rock burst problem is often monitored according to the AE signal in practical engineering. In the PFC model, when the stress between particles is greater than the flat joint model contact strength, the fracture occurs, that is, an AE hit occurs (Zhang et al. 2018). Therefore, the acoustic emission phenomenon can be simulated by writing fish language to monitor the fracture of the model.

It is shown that with the augment of stress–strain curve until the peak, the AE hits of numerical specimens presents three stages. In the first stage, stress less than point A, AE hits is almost zero; this step is in the elastic stage, and there isn't any crack in the sample. In the second stage, the stress is about between point A and point B. In this stage, AE hits is in a slowly increasing stage, which is due to the micro cracks in the model continuous expansion. In the third stage, after the B point, the AE



**Table 6** Failure pattern in models with different room's height and pillar wide

Room height (cm)	Pillar length (cm)		
	3	6	9
1	(a)	(b)	(c)
2	(d)	(e)	(f)
3	(g)	(h)	(i)
4	(j)	(k)	(l)
5	(m)	(n)	(o)
6	(p)	(q)	(r)



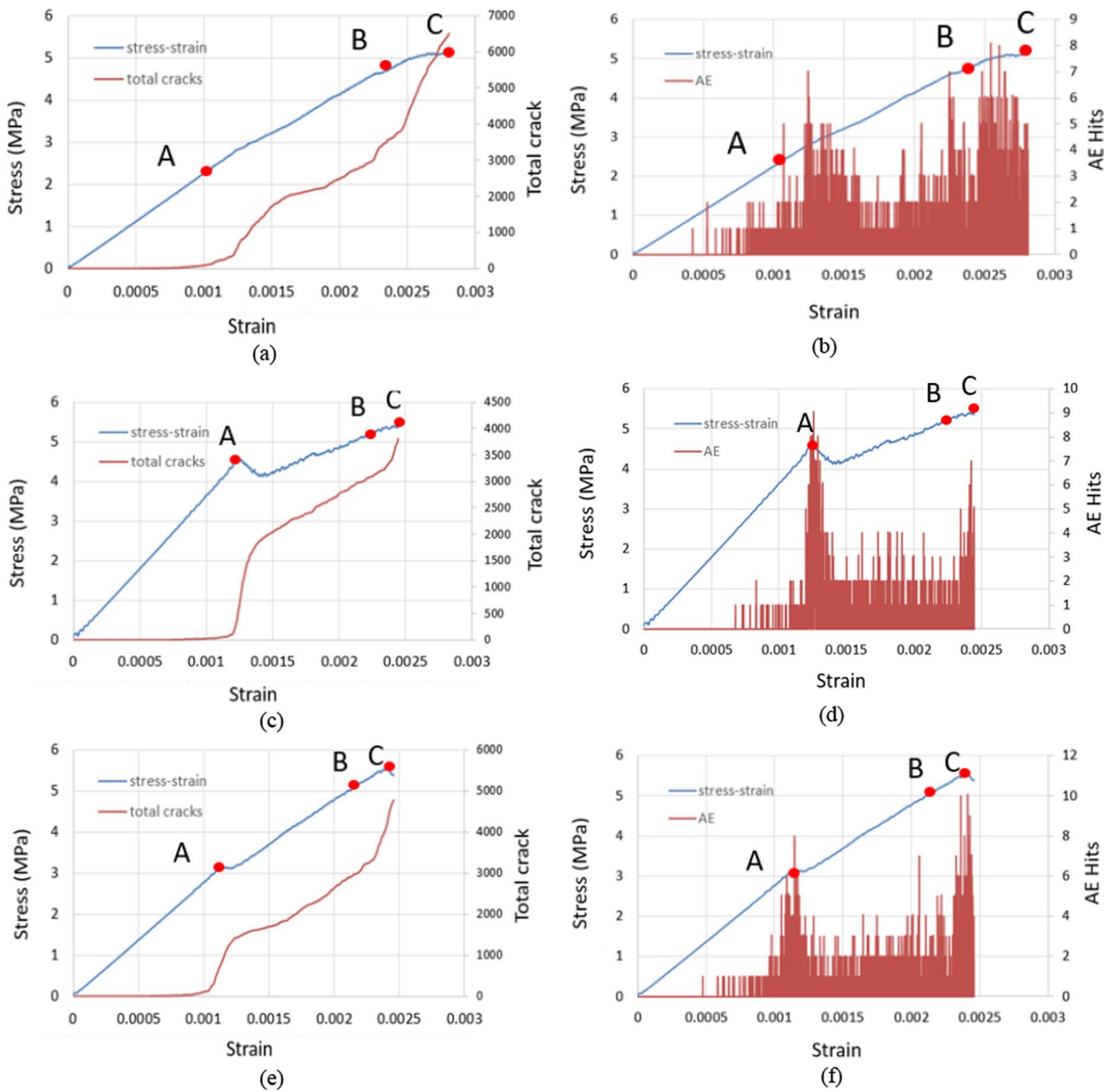


**Fig. 10** Stress and AE performance in the test simulation for three pillar wide, **a** stress–strain curve and cumulative crack number for pillar wide of 3 cm, **b** AE hits quantities across the strain curve for pillar wide of 3 cm, **c** stress–strain curve and cumulative crack number for pillar wide of 6 cm, **d** AE

hits quantities across the strain curve for pillar wide of 6 cm, **e** stress–strain curve and cumulative crack number for pillar wide of 9 cm, **f** AE hits quantities across the strain curve for pillar wide of 9 cm; roof height was 1 cm

hits increase rapidly, because the rock almost enters its bearing limit and the crack propagation speed is very fast. Generally, the maximum value of AE is near the peak value. When the roof height is

the same, different pillar wide led to a significant change in the maximum AE hits. These trends were occurred in other roof height (for example roof height of 6 cm in Fig. 11).

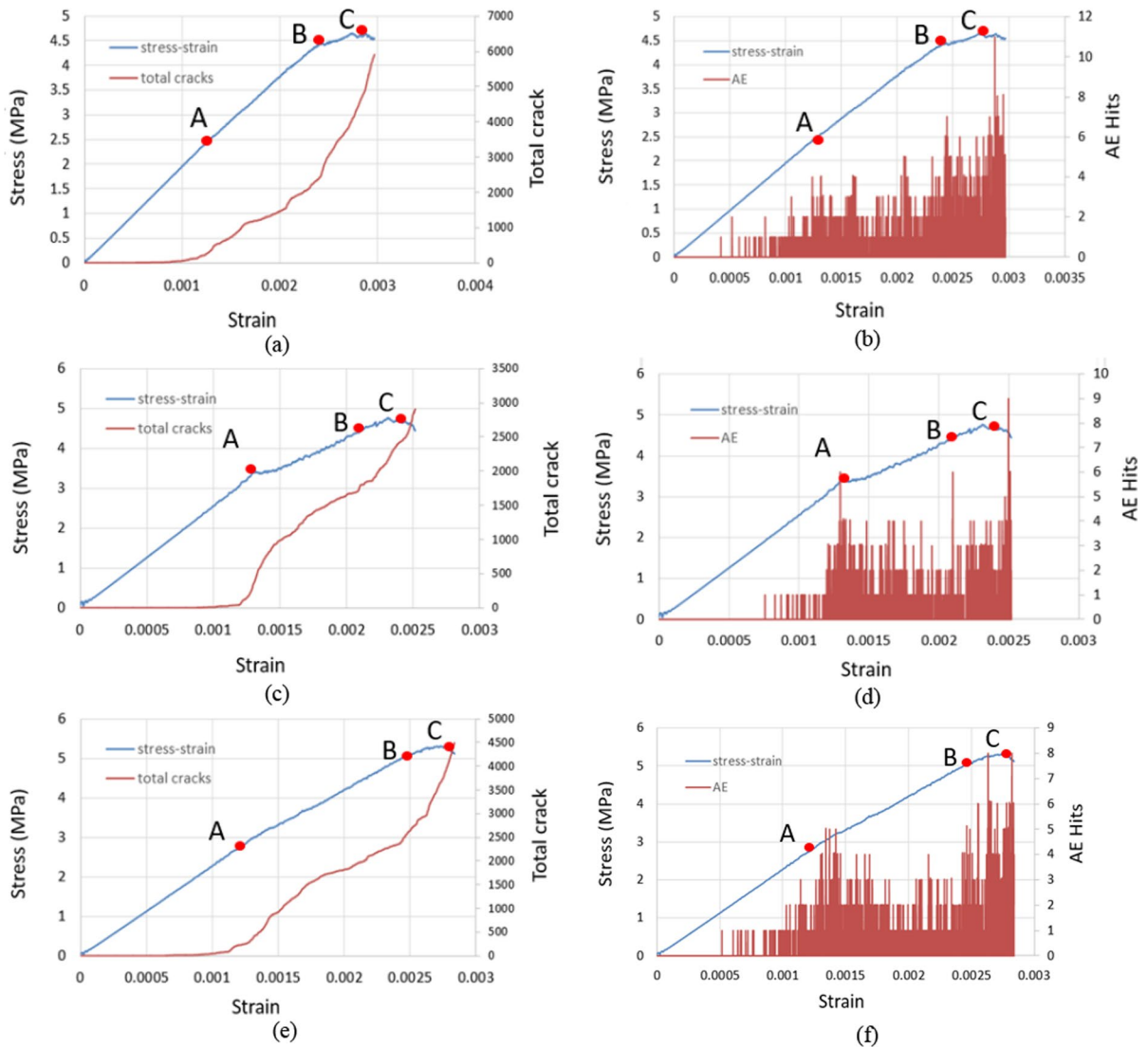


**Fig. 11** Stress and AE performance in the test simulation for three pillar wide, **a** stress–strain curve and cumulative crack number for pillar wide of 3 cm, **b** AE hits quantities across the strain curve for pillar wide of 3 cm, **c** stress–strain curve and cumulative crack number for pillar wide of 6 cm, **d** AE

hits quantities across the strain curve for pillar wide of 6 cm, **e** stress–strain curve and cumulative crack number for pillar wide of 9 cm, **f** AE hits quantities across the strain curve for pillar wide of 9 cm; roof height was 6 cm

### 3.4.5 Effect of pillar wide and rooms height on the final strength of models

Figure 12 shows the influence of pillar width on the model strength. Mentioned figure was introduced for different room’s height of 1 cm, 2 cm, 3 cm, 4 cm, 5 cm and 6 cm. In constant room’s height, the model strength increased by increasing the pillar wide. This is due to high tensile force concentration in pillar with

lower wideness (Fig. 7). Figure 12b show the effect of room’s height on the model strength. This figure was presented for different pillar wide of 3 cm, 6 cm, and 9 cm. In constant pillar wide, the model strength decreased by increasing the room’s height. This is due to high tensile force concentration in room with higher height (Fig. 6). By comparing Figs. 4 and 12, it’s clear that the numerical model strength was similar to experimental one.

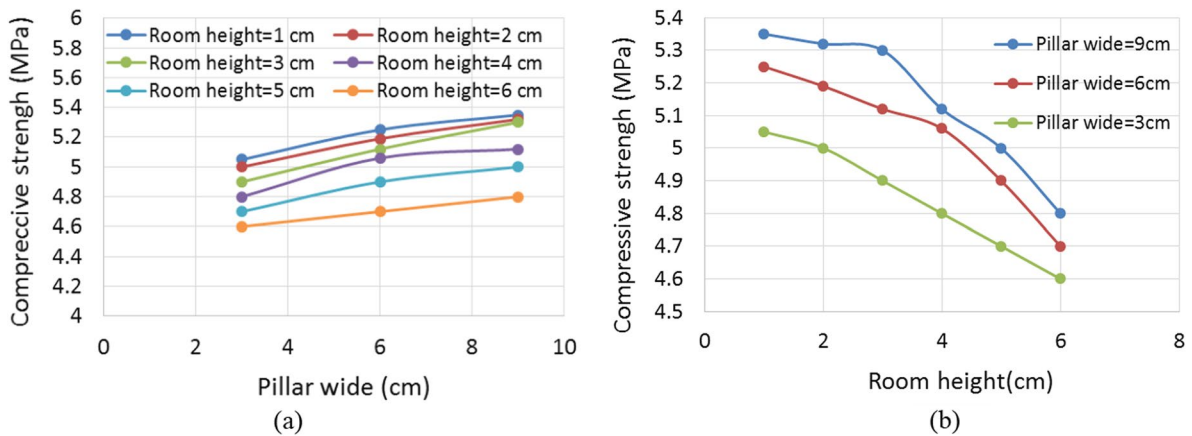


**Fig. 12** **a** Effect of pillar wide on the model strength, **b** Effect of room's height on the model strength

#### 4 Discussion

The pillar failure having various width-to-height ratios was studied by both of the experimental test and numerical simulation. In fixed pillar height, pillar width was altered from 3 to 9 cm with increment of 3 cm. Conceptual PFC<sup>2D</sup> models of pillar have been modeled with the loading being exerted via determined displacements as if they were exposed to uniaxial loading condition. The pure tensile cracks were initiated at the end of elastic stages while the shear cracks were developed through the rock pillar when residual strength is reached. As a result of merging of the cracks induced throughout the process of fracturing, the mixed mode shear-tensile cracks show the real generation of major fractures in the field. The growth of destroyed pillar hourglasses is highlighted by the plot of the broken zones within the rock pillar (Table 6). It is obvious that pillars with low w/h ratio treat in a brittle manner than pillars with high w/h ratio, where the procedure of degradation is related with pillar strain-softening (Figs. 10 and 11). For slender pillars, a considerable decline of load-carrying sufficiency associated with the nucleation of shear fractures into the pillar core is seen. On the other hand, a remarkable growth of capacity is demonstrated where failure is caused by little fractures.

The outcomes reported in current research indicate that the growth of thoroughgoing shear fractures, displaying decrease in loading capacity, happens for less width-to-height ratios (less than 1). In contrast,

for upper w/h ratios (more than 1), shear bands were developed in the pillar sidewalls with the progress of pillar hourglassing. Secondly, confined growing fracturing and lateral spalling happens, possibly consist of displacement of huge blocks, though commonly without compromising the loading capacity of the pillar. These outcomes are consistent with existing anticipations made by various modeling procedures. (Fang et al. 2002; Elmo et al. 2010; Cammaratal et al. 2023).

The displacement of the coal pillar can be divided into four phases: the primary compression phase, the stable rise phase, the mutation phase and the rapid rise phase. The fracture process of the coal pillar indicates that both of lower and upper parts of the edge begin to deface first, then the deformation is transferred to the corner of the coal pillar. The inconstancy in the coal pillar starts close by the edge and rouses inward, gently. Transferring from brittle behaviour to strain-softening manner was happened with enhancing the pillar aspect ratio.

#### 5 Conclusion

This paper investigates the effects of pillar wide and room's height on the failure mechanism of model using experimental test and numerical simulation. For this purpose, firstly gypsum specimens with dimension of 15\*15\*5 cm containing two neighboring rooms and one pillar were prepared. Pillar wide were

3 cm, 6 cm and 9 cm. In each pillar wide, the roof height was 1 cm, 2 cm, 3 cm, 4 cm, 5 cm, and 6 cm. The results show that:

- The compressive force chain was concentrated in the center of pillar while tensile force was concentrated in the pillars wall. In constant pillar wide, the tensile force concentration at the pillar wall increased by increasing the room's height. In constant room's height, the tensile force concentration was decreased by increasing the pillar wide.
- Two different failure patterns were observed in the model. In the first stage, two tensile fractures were developed from room edge and propagated parallel to loading axis till coalescence with model boundary. In the second stage, mixed tensile-shear cracks were developed through the rock pillar. the failure intensity decreased by increasing the pillar wide. The failure intensity increased by increasing the rooms height.
- In constant pillar wide, the shear cracks increased in the model by increasing the room's height. Also, in constant room's height, the shear bands developed in the model by increasing the pillar wide.
- It is shown that with the augment of stress–strain curve until the peak, the AE hits of numerical specimens presents three stages. In the first stage, AE hits is almost zero; this step is in the elastic stage, and there isn't any crack in the sample. In the second stage, AE hits is in a slowly increasing stage, which is due to the micro cracks in the model continuous expansion. In the third stage, the AE hits increase rapidly, because the rock almost enters its bearing limit and the crack propagation speed is very fast. Generally, the maximum value of AE is near the peak value. When the roof height is the same, different pillar wide led to a significant change in the maximum AE hits.
- In all the configurations, the angles of micro cracks varied from 75° to 105° degree. It means that the variations of pillar wide and rooms height have not any effect on the fracture angle.
- In constant room's height, the compressive strength and elastic modulus of the rock pillar are increased by increasing the pillar wide. In constant pillar wide, the model strength are decreased by increasing the room's height.

- The experimental test and numerical simulation show the similar results.

#### Declarations

**Conflict of interest** The authors have not any conflict of interest.

**Open Access** This article is licensed under a Creative Commons Attribution 4.0 International License, which permits use, sharing, adaptation, distribution and reproduction in any medium or format, as long as you give appropriate credit to the original author(s) and the source, provide a link to the Creative Commons licence, and indicate if changes were made. The images or other third party material in this article are included in the article's Creative Commons licence, unless indicated otherwise in a credit line to the material. If material is not included in the article's Creative Commons licence and your intended use is not permitted by statutory regulation or exceeds the permitted use, you will need to obtain permission directly from the copyright holder. To view a copy of this licence, visit <http://creativecommons.org/licenses/by/4.0/>.

#### References

- Bieniawski ZT (1968) The effect of specimen size on compressive strength of coal. *Int J Rock Mech Min Sci* 5(4):325–335
- Bobet A, Einstein HH (1998) Fracture coalescence in rock-type materials under uniaxial and biaxial compression. *Int J Rock Mech Min Sci* 35:863–889
- Bogert H, Jung SJ, Lim HW (1997) Room and pillar stope design in highly fractured area. *Int J Rock Mech Min Sci* 34(10):45–159
- Brady BGH, Brown ET (1985) *Rock mechanics for underground mining*. Allen&Unwin, Boston, Mass
- Cammaratal G, Elmo D, Brasile S (2023) Modelling of progressive failure mechanism of mine pillars. *IOP Conf Series Earth Environ Sci* 11(24):67–89. <https://doi.org/10.1088/1755-1315/1124/1/012099>
- Chen ZH, Tang CA, Huang RQ (1997) A double rock sample model for rockbursts. *Int J Rock Mech Min Sci* 34(6):991–1000
- Chen SL, Lee SC, Gui MW (2009) Effects of rock pillar width on the excavation behavior of parallel tunnels. *Tunn Undergr Space Technol* 24:148–154
- Elmo D, Stead D (2010) An integrated numerical modelling–discrete fracture network approach applied to the characterization of rock mass strength of naturally fractured pillars. *Rock Mech Rock Eng* 43(1):3–19
- Esterhuizen GS (2006) An evaluation of the strength of slender pillars. In: Yernberg WR (ed) *Transactions of society for mining, metallurgy, and exploration*, vol 320, pp

- 69–76. Society for Mining, Metallurgy, and Exploration, Littleton
- Fan J, Chen J (2019) A stress model reflecting the effect of the friction angle on rockbursts in coal mines. *Geomech Eng* 18(1):121–134
- Fang Z, Harrison JP (2002) Numerical analysis of progressive fracture and associated behaviour of mine pillars by use of a local degradation model. *Trans Inst Min Metall* 111:59–72
- Gao W (2018) Influence of interaction between coal and rock on the stability of strip coal pillar. *Geomech Eng* 16(2):66–78
- Ghasemi E, Shahriar K (2012) A new coal pillars design method in order to enhance safety of the retreat mining in room and pillar mines. *Saf Sci* 50(3):579–585
- Ghasemi E, Ataei M, Shahriar K (2014) An intelligent approach to predict pillar sizing in designing room and pillar coal mines. *Int J Rock Mech Min Sci* 65:86–95
- Gonzalez-Nicieza C (2006) A comparative analysis of pillar design methods and its application to marble mines. *Rock Mech Rock Eng* 39(5):421–444
- Jin Y (2018) Experimental investigation of the mechanical behaviors of grouted crushed coal rocks under uniaxial compression. *Geomech Eng* 16(3):77–89
- Kaiser PK, Tang CA (1998) Numerical simulation of damage accumulation and seismic energy release during brittle rock failure. Part II: Rib pillar collapse. *Int J Rock Mech Min Sci* 35(2):123–134
- Li J (2020) The plastic zone in surrounding rocks Arabian Journal of The coal pillar design method for a deep mining roadway based on the shape of the plastic zone in surrounding rocks. *Arabian J Geosci* 13(12):1005–1008
- Li YH, Nan SQ (2005) Stability of boundary pillars for transition from open pit to underground mining. *Chin J Rock Mech Eng* 24(2):278–283
- Liu H (2021) Study on mechanical properties and damage features of rock-Coal-rock combination models with defects and fillings. *Geomech Eng* 27(3):165–173
- Liu J, He M (2021) Force change of the gravel side support during gangue heaping under a new non-pillar-mining approach. *Geomechan Eng* 27(1):88–99
- Liu MY, Xu CY (2000) Stability analysis of pillars in mined out area. *Min Metall Eng* 20(1):20–22
- Lunderand PJ, Pakalnis RC (1998) Determination of the strength of hard rock mine pillars. *World Min Express* 4:24–28
- Mortazavi A, Hassani FP, Shabani M (2009) A numerical investigation of rock pillar failure mechanism in underground openings. *Comput Geotech* 36(5):691–697
- Murali Mohan G, Sheorey PR, Kushwaha A (2001) Numerical estimation of pillar strength in coal mines. *Int J Rock Mech Min Sci* 38:1185–1192
- Potyondy DO (2015) The bonded-particle model as a tool for rock mechanics research and application: current trends and future directions. *Geosyst Eng* 18(1):1–28
- Potyondy DO, Cundall PA (2004) A bonded-particle model for rock. *Int J Rock Mech Min Sci* 41:1329–1364
- Potyondy DO (2012) A flat-jointed bonded-particle material for hard rock. Paper presented at the 46th U.S. Rock Mechanics/Geomechanics Symposium, Chicago
- Potyondy DO (2017) Simulating perforation damage with a flat-jointed bonded-particle material. Paper presented at the 51st US Rock Mechanics/Geomechanics Symposium, San Francisco, California, USA.
- Qiu P, Wang J (2019) Rock burst criteria of deep residual coal pillars in an underground coal mine: a case study. *Geomech Eng* 19(6):111–123
- Qu X, Chen SH, Yi D (2021) Experimental study of the strip coal pillar models failure with different roof and floor conditions. *Arch Min Sci* 66(3):475–490. <https://doi.org/10.24425/ams.2021.138601>
- Reyes O, Einstein HH (1991) Failure mechanism of fractured rock—a fracture coalescence model. In: Proceedings of 7th Congress of the ISRM, Tokyo, Japan, 1:333–340
- Sarfarazi V, Abharian S, Ghorbani A (2021) Physical test and PFC modelling of rock pillar failure containing two neighboring joints and one hole. *Smart Struct Syst* 27(1):99–111
- Shen B, Stephansson O, Einstein HH, Ghahreman B (1995) Coalescence of fracture under shear stresses in experiments. *J Geophys Res* 100:725–729
- Sun W, Du H (2019) Experimental study of crack propagation of rock-like specimens containing conjugate fractures. *Geomech Eng* 17(4):35–47
- Suorineni FT, Kaiser PK (2011) Mining of ore bodies under shear loading part 1—case histories. *Min Technol Trans Inst Min Metall A* 120(3):137–147
- Suorineni FT, Mgumbwa JJ, Kaiser PK (2014) Mining of ore-bodies under shear loading part 2—failure modes and mechanisms. *Min Technol Trans Instit Min Metall A* 123(4):240–249
- Takeuchi K (1991) Mixed-mode fracture initiation in granular brittle materials, M.S. Thesis, Massachusetts Institute of Technology, Cambridge
- Wang ZQ, Li HF (2010) Numerical calculation method for shear safety coefficient of mine pillar. *J Min Saf Eng* 27(2):277–280
- Wang XJ, Feng X, Yang TB (2012) Reasonable width calculation and analysis of artificial pillar in deep mining. *J Min Saf Eng* 29(1):54–59
- Yang MC (2005) Study on size design method of pillars. *Min Technol* 5(3):10–12
- Zhang Q, Wang X, Tian L (2018) Analysis of mechanical and acoustic emission characteristics of rock materials with double-hole defects based on particle flow code. *Shock Vib* 32(1):23–35
- Zhong YW (2012) Safety pillar thickness determination and local monitoring in Wengfu phosphate. *Min Eng Res* 27(3):28–33

**Publisher's Note** Springer Nature remains neutral with regard to jurisdictional claims in published maps and institutional affiliations.